Title: Online 4D ultrasound guidance for real-time motion compensation by MLC tracking

By-line: Online 4D ultrasound-guided MLC tracking

5

Authors:

Svenja Ipsen*
10   Institute for Robotics and Cognitive Systems,
            University of Luebeck,
            23562 Luebeck, Germany

            * Corresponding author – Contact details:
15   Institute for Robotics and Cognitive Systems, University of Luebeck
            Ratzeburger Allee 160
            23562 Luebeck, Germany

            Phone: +49 451 3101 5217
20   Email: ipsen@rob.uni-luebeck.de

Ralf Bruder
            Institute for Robotics and Cognitive Systems,
            University of Luebeck,
25   23562 Luebeck, Germany

Rick O'Brien
            Radiation Physics Laboratory, Sydney Medical School,
            University of Sydney,
30   NSW 2006, Australia

Paul J Keall
            Radiation Physics Laboratory, Sydney Medical School,
            University of Sydney,
35   NSW 2006, Australia

A Schweikard
            Institute for Robotics and Cognitive Systems,
            University of Luebeck,
40   23562 Luebeck, Germany

Per R Poulsen
            Department of Clinical Medicine,
            Aarhus University
45   and
            Department of Oncology,
            Aarhus University Hospital,
            8000 Aarhus, Denmark

Title: Online 4D ultrasound guidance for real-time motion compensation by MLC tracking

By-line: Online 4D ultrasound-guided MLC tracking

Purpose: With the trend in radiotherapy moving towards dose escalation and hypofractionation, the need for highly accurate targeting increases. While MLC tracking is already being successfully used for motion compensation of moving targets in the prostate, current real-time target localization methods rely on repeated x-ray imaging and implanted fiducial markers or electromagnetic transponders rather than direct target visualization. In contrast, ultrasound imaging can yield volumetric data in real-time (3D + time = 4D) without ionizing radiation. We report the first results of combining these promising techniques – online 4D ultrasound guidance and MLC tracking – in a phantom.

Methods: A software framework for real-time target localization was installed directly on a 4D ultrasound station and used to detect a 2 mm spherical lead marker inside a water tank. The lead marker was rigidly attached to a motion stage programmed to reproduce nine characteristic tumor trajectories chosen from large databases (five prostate, four lung). The 3D marker position detected by ultrasound was transferred to a computer program for MLC tracking at a rate of 21.3 Hz and used for real-time MLC aperture adaption on a conventional linear accelerator. The tracking system latency was measured using sinusoidal trajectories and compensated for by applying a kernel density prediction algorithm for the lung traces. To measure geometric accuracy, static anterior and lateral conformal fields as well as a 358° arc with a 10 cm circular aperture were delivered for each trajectory. The two-dimensional (2D) geometric tracking error was measured as the difference between marker position and MLC aperture center in continuously acquired portal images. For dosimetric evaluation, VMAT treatment plans with high and low modulation were delivered to a biplanar diode array dosimeter using the same trajectories. Dose measurements with and without MLC tracking were compared to a static reference dose using 3%/3 mm and 2%/2 mm γ-tests.

Results: The overall tracking system latency was 172 ms. The mean 2D root-mean-square tracking error was 1.03 mm (0.80 mm prostate, 1.31 mm lung). MLC tracking improved the dose delivery in all cases with an overall reduction in the γ-failure rate of 91.2% (3%/3 mm) and 89.9% (2%/2 mm) compared to no motion compensation. Low modulation VMAT plans had no (3%/3 mm) or minimal (2%/2 mm) residual γ-failures while tracking reduced the γ-failure rate from 17.4% to 2.8% (3%/3 mm) and from 33.9% to 6.5% (2%/2 mm) for plans with high modulation.

Conclusions: Real-time 4D ultrasound tracking was successfully integrated with online MLC tracking for the first time. The developed framework showed an accuracy and latency comparable with other MLC tracking methods while holding the potential to measure and adapt to target motion, including rotation and deformation, non-invasively.

1. INTRODUCTION

The fundamental goal of radiation therapy is to maximize the dose to the treatment target while minimizing the dose to the surrounding healthy tissue. Technological advancements such as volumetric arc therapy (VMAT) or stereotactic ablative body radiotherapy (SABR) have led to improved dose distributions with steeper gradients and better sparing of organs-at-risk. Due to the current trend towards dose escalation and hypofractionation, the need for highly accurate targeting increases. This is especially challenging for organs and structures affected by motion.[1] Uncompensated motion can lead to a substantial loss of target coverage and dose smearing, impairing treatment quality.[2–4] As a consequence, intra-fractional motion compensation is a field of active research consisting of two major aspects: real-time target localization and treatment adaptation.

Adaptation of the treatment beam can be achieved by gating or tracking methods. While gating can be implemented on most clinical linear accelerators, it can prolong treatment time considerably and is mainly suited for periodic motion. Active beam steering, i.e. tracking, ideally does not add treatment time and is currently commercially available in the robotic CyberKnife system (Accuray, Sunnyvale, CA)[5] and the Vero gimbal system (BrainLab, Germany and Mitsubishi Heavy Industries, Japan)[6]. These systems are highly specialized and complex and therefore not nearly as common as conventional gantry-based accelerators. In an effort to integrate tracking into clinical routine, Keall *et al.* introduced MLC tracking in 2001.[3] It was successfully used for prostate tracking in a first clinical trial in 2013[7] and for lung SBRT at the end of 2015.[8] After being clinically demonstrated, MLC tracking is likely to become commercially available in the future and move towards widespread clinical utilization. MLC tracking has the unique potential to account not only for rigid target shifts but also for rotational motion and target deformations.[9]

The current standard for real-time target localization is the use of external or internal surrogate markers. External markers monitored with infrared cameras can provide a superficial breathing curve which is assumed to be correlated to the internal target motion. In the CyberKnife system, this method is extended with internal position data. Metal fiducials are implanted close to the target, imaged with kV-imagers and correlated to the external breathing curve, providing a more accurate correlation model.[10] However, the model-based approach is prone to "unexpected" motion that was not part of the model-building process and aperiodic shifts. A localization technique fully based on internal markers is available with the Calypso system (Varian Medical Systems, Palo Alto, CA), where electromagnetic transponders are implanted

3

around the target and continuously monitored by external antennas at 25 Hz.[11] All of the aforementioned methods share the common drawback of relying on surrogate signals, thus not measuring the actual target position. A high tracking accuracy requires the invasive implantation of markers and, in the case of the CyberKnife and the Vero gimbal system, also additional imaging dose to the patient.

110   Imaging modalities such as magnetic resonance imaging (MRI) or ultrasound might solve these problems as they provide superior soft tissue contrast compared to x-ray-based methods and a high temporal resolution. MRI-guidance is being thoroughly investigated with one commercial system on the market[12] and several research groups working on the integration of MRI into a radiotherapy setup[13–15]. It provides volumetric images with highest anatomical quality, however at the cost of a much higher system complexity and much lower temporal resolution.[16]

115   In contrast, modern ultrasound systems can visualize entire volumes in real-time with high frame rates. In this paper, we define the term "4D" as time-resolved, three-dimensional volumes acquired (and visualized) in real-time. Different methods for target localization in 4D ultrasound are currently under investigation. Registration-based approaches can yield an accuracy below 2 mm and account for deformation but at the cost of high computation times in the range of seconds to minutes prohibiting real-time motion compensation.[17–19] Harris *et al*. demonstrated 4D speckle

120 tracking in a phantom using a mechanical sweeping probe with an acquisition frequency of 1-2 Hz and sub-millimeter accuracy.[20, 21] Yet, Lediju-Bell *et al.* showed in 2012 that a minimum sampling rate of 4-12 Hz is required to accurately measure respiratory or cardiac motion.[22]

Despite showing promising results, all of these studies were performed offline on previously acquired data and have not been tested in a realistic tracking scenario. To the best of our knowledge, only one group has reported on online

125 ultrasound tracking of respiratory motion. Schwaab *et al.* used a pseudo-3D ultrasound transducer with two perpendicular 2D planes to measure target motion and actively steer a proton beam.[23] With a total system latency of about 200 ms they reported an accuracy of 4.8 mm in a phantom when compared to PET imaging.[24]

In this study, we describe the world-first online 4D ultrasound-guided MLC tracking experiment with a direct communication link between the ultrasound system and the MLC controller of a linear accelerator. By combining two of

130 the most promising techniques for treatment adaptation and target localization we hope to demonstrate the feasibility of using ultrasound for intra-fractional motion compensation with widespread usability in conventional radiotherapy systems.

2. MATERIALS AND METHODS

135   **2.1 Tracking system**

4

The tracking system as illustrated in Figure 1 consists of two major components: (1) A commercially available ultrasound station modified for online tracking and data streaming and (2) an MLC tracking prototype system integrated with a linear accelerator. Data transfer between both systems was realized via UDP network communication.

Online 4D ultrasound target localization was performed on a Vivid 7 dimension (General Electrics, Fairfield, CT) with a cardiovascular 3V matrix array probe using the second harmonic 2.0/4.0 MHz mode. To be able to record and process the volumetric data, a special client/server framework was designed allowing the installation of custom applications directly on the ultrasound station. This is crucial to circumvent the bottleneck of data transfer via network, which can cause delays of up to 100 ms (data size ~1 MB per volume).

For target localization, a maximum intensity search was used to find a phantom marker in an ultrasound volume. After a cluster of bright voxels was located within the volume, the neighboring area was interpolated using splines and the resulting marker position was found at the maximum value of the interpolated space. For more complex targets, e.g. soft-tissue tumors, template matching was also implemented although not used in this study. Template matching calculates the squared difference between the observed volume and a previously captured patient-specific template. The maximum similarity (minimum difference) over all positions indicates the target location. In our experiments, we chose the maximum intensity search since it detects a spherical marker in a water tank with the highest possible accuracy in less than 5 ms. Template matching would be used in real anatomical data with more scattering structures to track, adding about 15 ms computation time. The target position was sent from the ultrasound station to the MLC tracking computer in real-time via UDP messages.

MLC tracking experiments were conducted on a Trilogy linear accelerator with a 120 leaf Millennium MLC equipped with a PortalVision IAS500 portal imager (Varian Medical Systems, Palo Alto, CA).
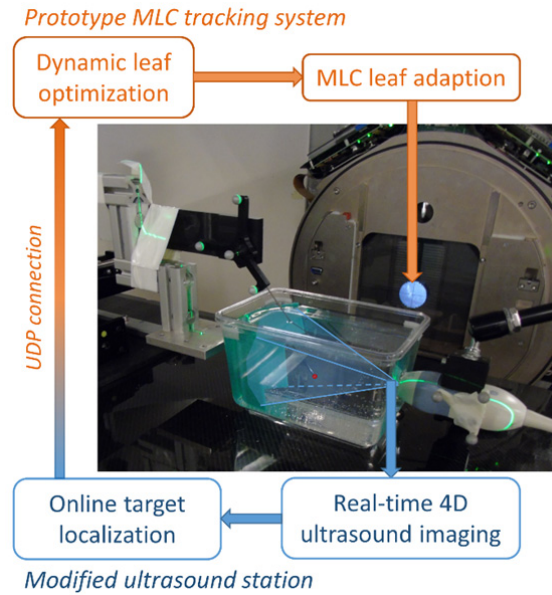
5

Figure 1: Workflow of ultrasound-guided MLC tracking using an ultrasound station modified for online image processing and data transfer and a prototype MLC tracking system for real-time leaf optimization.

2.2 Experimental setup

As shown in Figure 2, the ultrasound phantom consisted of a water bath with damping material opposite to the ultrasound transducer to avoid acoustical interference artefacts and a spherical lead marker (Ø 2 mm) attached to a plastic pointer. The phantom was placed on the treatment couch with the transducer pressed against one side using a tripod and coupling gel. The ultrasound station calculated distances based on the assumed mean speed of sound in soft tissues (1540 m/s). To avoid systematic errors introduced by the different speed of sound in pure water (1480 m/s), the phantom was filled with a 6.5% saline solution as higher salinity increases the speed of sound.[25]
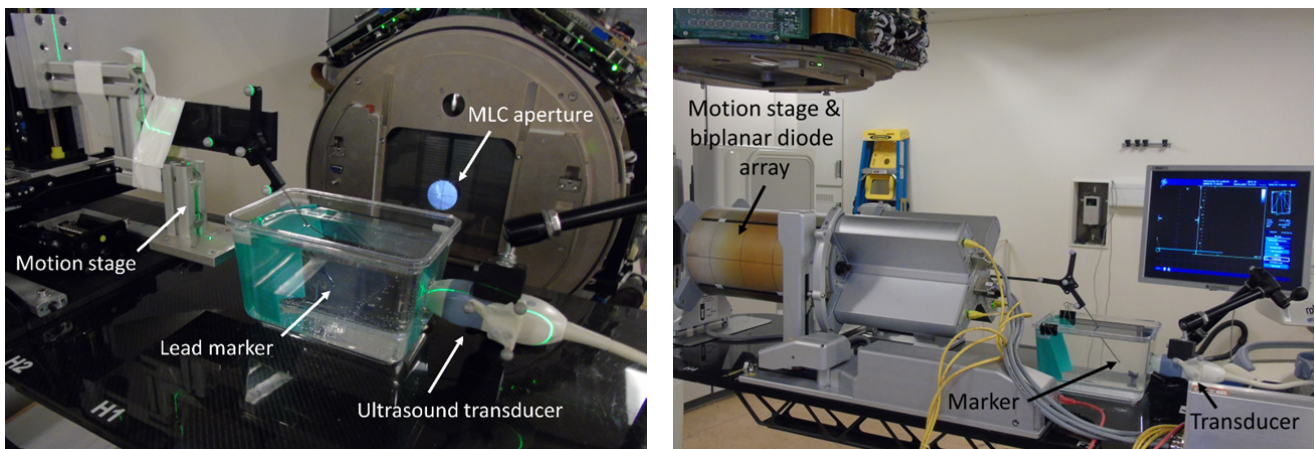

Figure 2: (a) Setup for geometric accuracy assessment of online ultrasound-guided MLC-tracking. A lead sphere in a water bath was moved by a motion stage, detected with 4D ultrasound and its position sent to the MLC tracking software which calculated and updated the MLC

6

Motion traces

The main aim of this study was to investigate ultrasound-guided MLC tracking by generating data that are comparable with current state-of-the-art target localization methods such as electromagnetic transponders or kV imaging. Therefore, we adapted the experimental setup from previous studies[26–28] and used the same prostate and lung tumor trajectories, carefully selected from large databases[29, 30] in order to cover a wide range of motion types as summarized in Table 1 (lung – "typical", high-frequency, predominant left–right, baseline variations; prostate – stable, high-frequency, continuous drift, persistent excursion, transient excursion). More details on the utilized traces can be found in previous publications.[27, 31] Prostate motion was chosen because highly complex motion can occur in some cases while lung tumor trajectories show especially large magnitudes and high frequencies of quasi-periodic motion well-suited to test tracking and prediction performance.

Table 1: Motion trajectories used for geometric and dosimetric tracking accuracy measurements.

|		Motion range (mm)		
Region	Trajectory	S-I	A-P	L-R
Prostate	High frequency	8.3	10.8	1.5
	Continuous drift	8.2	7.5	2.0
	Persistent	5.2	8.7	1.1
	Stable	1.4	0.8	0.7
	Transient	6.0	14.5	1.1
Lung	Baseline shift	5.6	17.0	18.1
	High frequency	17.8	2.4	1.2
	Predominantly LR	1.7	7.7	21.4
	Typical	11.5	2.5	1.9

Latency and geometric accuracy

Tracking latency and geometric accuracy were measured using a 10cm diameter circular field with the MLC leaves aligned in the superior-inferior (SI) direction. A beam energy of 6MV was used. As shown in Figure 2a, the pointer with the lead sphere was mounted on a programmable motion stage[32] and submerged in the water tank. A simple isocenter alignment of the sphere based on orthogonal MV images was performed in accordance with previous experiments, e.g. by Ravkilde *et al.*[28] By moving the motion stage along the main axes the ultrasound system was calibrated to transform the ultrasound coordinates into the treatment coordinates of the accelerator. MV portal images showing the lead sphere and the circular

7

MLC aperture were continuously acquired at 12.9 Hz by an AS500 portal imager (Varian) during the experiments. The pixel size in the isocenter was 0.44 mm.

For latency estimation, the motion stage performed sinusoidal motions with 12 mm peak-to-peak amplitude and period lengths of 2 s, 3 s, 4 s, 5 s and 6 s. The latency of the tracking chain was determined as the time lag between the lead sphere motion and the MLC aperture motion in portal image series of 2 min duration (see Figure 3). The mean latency for the five period lengths was reported. Since the image acquisition and target localization time depends strongly on the geometry of the imaged volume, latency was investigated for three different volume settings. The smallest volume, acquired using the in-built zoom function of the ultrasound station, covered a depth of 45 mm (at 130 mm target distance) and 8 by 6 degrees in the azimuthal and elevational direction. This 17 x 14 x 45 mm^3 volume was updated at a frame rate of 250 Hz. To cover an increasing extent of motion, a medium and large volume with 30 by 22 degrees and 30 by 46 degrees (68 mm x 50 mm and 68 mm x 105 mm, both measured at 130 mm depth) were acquired covering 170 mm in depth with frame rates of 21.3 Hz and 17.8 Hz, respectively. For the subsequent experiments, the medium volume size was chosen as a good compromise between motion range, resolution and speed.

To measure geometric accuracy, the motion stage was programmed with the prostate and lung trajectories (see previous section). For each trajectory, three treatment fields with 600 MU were delivered with 600 MU/min: static anterior, static lateral and a 358° arc. For lung motion, a kernel density estimation algorithm[33] was used to account for the estimated system latency. The treatment was started 20 s after the start of ultrasound tracking since the motion prediction algorithm needed a training data set of measured 3D ultrasound positions. No latency compensation by prediction was used for the prostate cases due to the irregular patterns of prostate motion.

In an offline analysis, the lead sphere and the circular MLC aperture were segmented in each portal image.[34] The 2D tracking error in beam's eye view was calculated as the difference between the marker position and the center of the circular MLC aperture for each portal image. The root-mean-square (rms) of the tracking error was determined for each treatment.
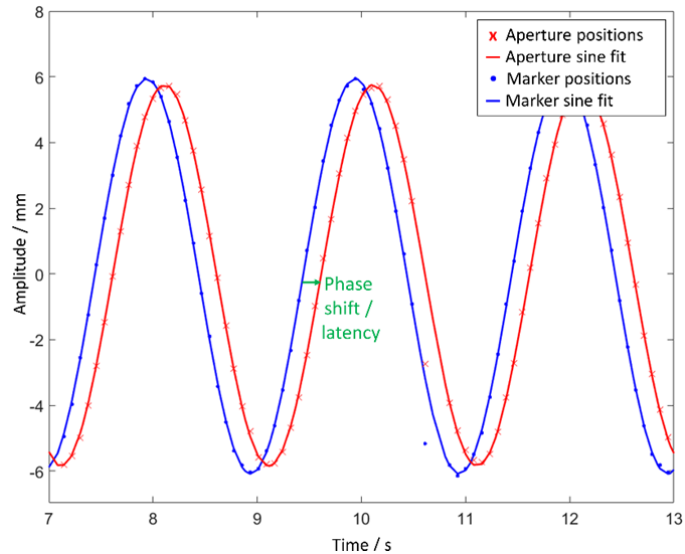
Figure 3: Latency estimation by calculating the phase shift between the sine functions fitted to the segmented position of the target marker (blue) and the circular MLC aperture (red) in continuous portal images.

Dosimetric accuracy

A dosimeter phantom (Delta4PT, ScandiDos, Sweden) with two orthogonal planar diode arrays encased in cylindrical
220 PMMA was mounted on a programmable motion stage (HexaMotion, ScandiDos) and used for measurements of the dosimetric accuracy. The lead sphere pointer was rigidly attached to the dosimeter and the ultrasound phantom was placed at the inferior end outside the treated region (Fig. 2a). The ultrasound system was again realigned with treatment room coordinates.

For each trajectory, VMAT treatment plans with high and low modulation were delivered once with MLC tracking
225 and once without. The plans were the same as used in the study by Keall *et al.*[27] Additionally, a reference dose was delivered to a static phantom for each of the four plans (two prostate, two lung). The dose distributions with and without MLC tracking were compared with the static dose using γ-tests with 3% and 2% dose difference and 3 mm and 2 mm distance to agreement (normalized to the static isocenter dose with a 10% low dose cutoff). The fraction of points failing the γ -test (the γ-failure rate) was recorded for each plan and each tumor trajectory.

230

3. RESULTS

The mean (and standard deviation) of the tracking system latency for the five sinusoidal motions was 184.6 ms (8 ms) for the large volume size, 172.2 ms (11 ms) for the medium volume and 95.5 ms (8 ms) for the smallest tracking volume. Since

9

the subsequent experiments were conducted with the medium volume setting, the prediction length for the lung traces

235 was set to 170 ms.

3.1 Geometric accuracy

Figure 4 shows the tracking results for two prostate and one lung tumor trajectory extracted from portal images. The mean Cartesian resolution of the ultrasound volume in the target area (depth ca. 130 mm) was 0.3 x 0.8 x 1.6 mm. The rms errors for all 27 experiments (nine trajectories, three fields) are summarized in Table 2. The overall tracking accuracy was

240 1.03 mm with a precision (standard deviation) of 0.3 mm. The lung traces, having a higher motion amplitude and frequency, showed a higher error of 1.31 mm compared with 0.80 mm for the prostate. Most prostate traces were tracked with sub-millimeter accuracy (the only exception being the high-frequency excursion) and 0.1 mm precision while the lung trajectories were tracked with sub-2-mm accuracy and 0.2 mm precision.

Visual inspection of the tracking results showed a constant systematic offset of -0.4 mm in the SI-direction

245 between the marker position and the MLC aperture center in all measurements (see Figure 4). It lies in the range of one MV imager pixel and could have been introduced by a misalignment that occurred during or after the initial calibration. Assuming that this error could be avoided with a more thorough calibration and a higher imager resolution, the offset was manually subtracted to investigate its impact on the tracking results. After offset correction, the overall tracking error was reduced to 0.85 mm (0.61 mm prostate, 1.16 mm lung).

250

Table 2: Mean tracking errors (rms) of ultrasound-guided MLC tracking for nine trajectories and three field types. A systematic offset was observed in the original measurements (see Figure 4) and corrected for retrospectively to assess its impact in the right part of the table.

| | | Mean tracking error (mm) | | | | | |
| | | No offset correction | | | With offset correction (-0.4 mm) | | |
Region	Trajectory	358° Arc	Static Lateral	Static Anterior	358° Arc	Static Lateral	Static Anterior
Prostate	High frequency	1.11	1.08	0.78	0.95	0.97	0.59
	Continuous drift	0.89	0.87	0.59	0.68	0.69	0.28
	Persistent	0.82	0.75	0.57	0.73	0.56	0.35
	Stable	0.97	0.81	0.72	0.75	0.53	0.41
	Transient	0.73	0.74	0.59	0.74	0.56	0.32
	Mean ± std	**0.80 ± 0.15**			**0.61 ± 0.19**		
Lung	Baseline shift	1.17	1.12	1.08	1.09	0.99	0.99
	High frequency	1.47	1.79	1.61	1.38	1.61	1.47
	Predominantly LR	1.03	1.08	1.27	0.92	0.86	1.18
	Typical	1.48	1.45	1.23	1.24	1.16	1.00
	Mean ± std	**1.31 ± 0.25**			**1.16 ± 0.24**		
All	**Mean ± std**	**1.03 ± 0.35**			**0.85 ± 0.38**		
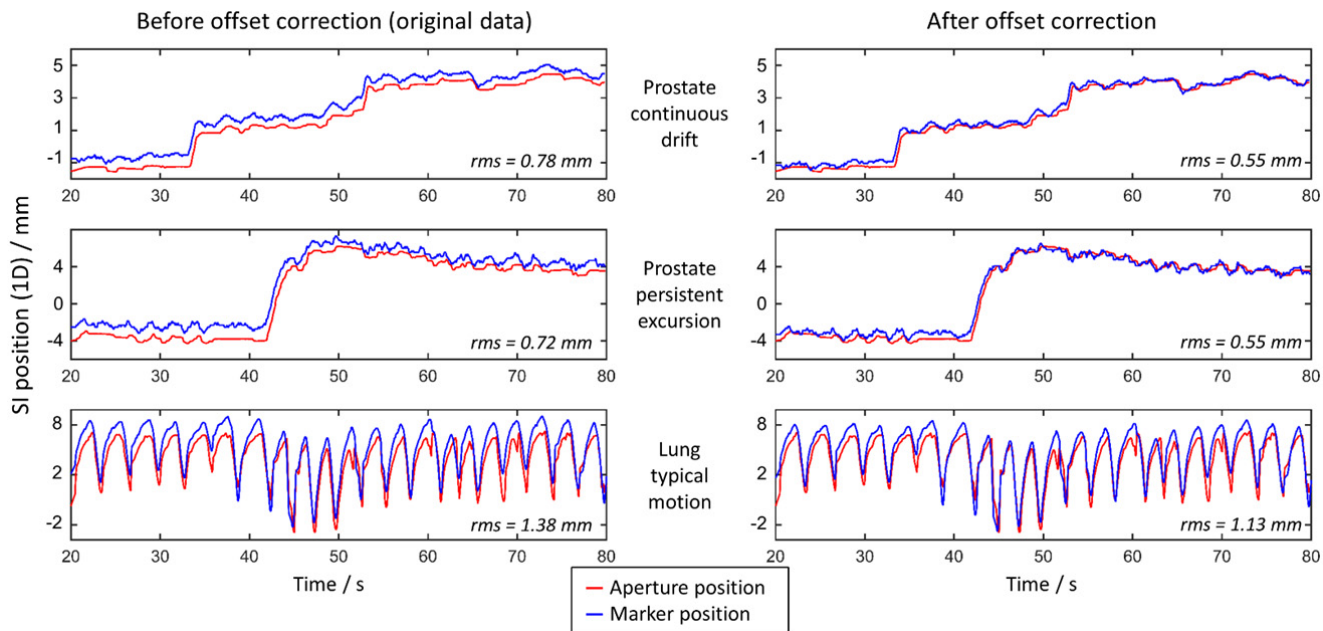
Figure 4: Geometric tracking accuracy. The tracking error was defined as the rms difference between the marker position (blue) and the MLC aperture center (red). A systematic offset was observed in the original measurements (left) and was corrected for retrospectively by manual subtraction (right). The numbers specify the mean 2D root-mean-square tracking error over all three treatment fields for each trajectory.

3.2 Dosimetric accuracy

The motion-induced γ-failure rates for the high-modulation VMAT plans are shown in Figure 5 with and without MLC tracking. Table 3 and Table 4 summarize all results of the 3%/3 mm and 2%/2 mm γ-tests.

11
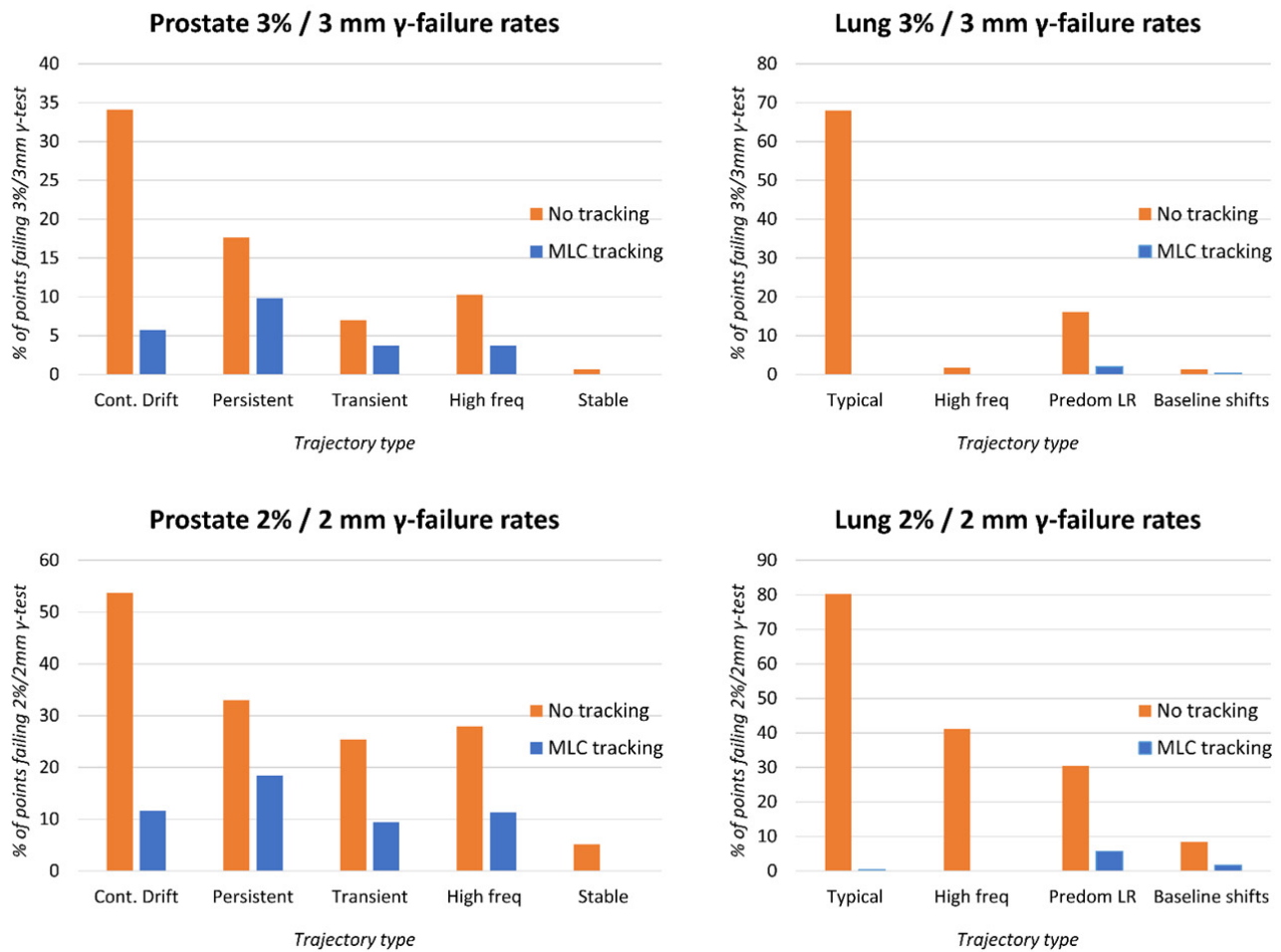
Figure 5: Dosimetric accuracy of ultrasound-guided MLC tracking. The percentage of dose values failing the 3%/3mm and 2%/2mm γ-test, with and without tracking, for the high-modulation VMAT plans and nine motion traces. Note that the y-scale is different for all four plots.

In all cases, MLC tracking improved the γ-failure rate substantially compared with the results without motion compensation. All low modulation plans had no remaining γ-failures above 2%/2 mm when tracking was applied, except for the *persistent excursion* prostate (0.2%) and *typical* lung (0.3%) traces in the 2%/2 mm test. Especially the *persistent excursion* prostate trace seemed to be more complicated to track than other traces as it resulted in the highest observed tracking failure rates of 9.8% (3%/3 mm) and 18.4% (2%/2 mm) for the high modulation plans. Without motion compensation, the *typical* lung trace caused the highest dose discrepancies with up to 86% (low modulation plan, 2%/2 mm γ-test).

For the high and low modulation lung plans combined, the failure rate in the 3%/3 mm γ-test was 0.3% with tracking compared with 19.9% without tracking and 1.0% compared with 38.0% in the 2%/2 mm test. For the combined prostate plans, 2.3% and 9.5% (3%/3 mm) and 5.1% and 22.0% (2%/2 mm) of the dose points failed with and without tracking, respectively. The overall improvement from plan delivery without motion compensation to real-time treatment adaptation was 91.2% for the 3%/3 mm and 89.9% for the 2%/2 mm γ-test. Improvements from tracking were generally

12

280 higher in the lung plans compared with the prostate. The VMAT plans with ultrasound-guided MLC tracking were delivered without beam holds and completed in the same time as the static and no-tracking plans.

Table 3: 3% / 3 mm γ-failure rates for nine trajectories and two degrees of modulated VMAT plans.

| | | 3% / 3 mm γ-failure rates in % | | | |
| | | High Modulation | | Low Modulation | |
Region	Trajectory	No tracking	MLC tracking	No tracking	MLC tracking
Prostate	High frequency	10.3	3.7	2.8	0.0
	Continuous drift	34.1	5.7	21.4	0.0
	Persistent	17.6	9.8	0.2	0.0
	Stable	0.7	0.0	0.0	0.0
	Transient	7.0	3.7	0.8	0.0
	Mean	**13.9**	**4.6**	**5.0**	**0.0**
Lung	Baseline shift	1.3	0.3	0.0	0.0
	High frequency	1.8	0.0	3.0	0.0
	Predominantly LR	16.1	2.0	1.4	0.0
	Typical	68.0	0.0	67.5	0.0
	Mean	**21.8**	**0.6**	**18.0**	**0.0**
All	**Mean**	**17.4**	**2.8**	**10.8**	**0.0**

Table 4: 2% / 2 mm γ-failure rates for nine trajectories and two degrees of modulated VMAT plans.

| | | 2% / 2 mm γ-failure rates in % | | | |
| | | High Modulation | | Low Modulation | |
Region	Trajectory	No tracking	MLC tracking	No tracking	MLC tracking
Prostate	High frequency	28.0	11.3	14.5	0.0
	Continuous drift	53.7	11.6	46.3	0.0
	Persistent	33.0	18.4	6.6	0.2
	Stable	5.1	0.0	0.8	0.0
	Transient	25.4	9.4	7.0	0.0
	Mean	**29.0**	**10.1**	**15.0**	**0.0**
Lung	Baseline shift	8.4	1.7	0.0	0.0
	High frequency	41.2	0.0	41.6	0.0
	Predominantly LR	30.4	5.7	16.8	0.0
	Typical	80.2	0.3	85.5	0.3
	Mean	**40.1**	**1.9**	**36.0**	**0.1**
All	**Mean**	**33.9**	**6.5**	**24.3**	**0.1**

285

4. DISCUSSION

In this study, real-time 4D ultrasound guidance was successfully integrated with a prototype MLC tracking system for online motion compensation for the first time. By using a custom ultrasound phantom and motion stages programmed

13

with different patient tumor traces, the system was characterized regarding its latency, geometric and dosimetric

290   accuracy.

The overall system latency includes image acquisition, target localization, transfer, waiting time before next leaf fitting, aperture optimization and travel time of the MLC leaves.[35] As the last two components are more or less constant (~56 ms)[35], the latency of the system is mainly determined by the target localization frequency (acquisition and detection). A smaller volume leads to less reconstructed ultrasound beams and thus a faster frame rate. The smallest

295   tracking volume of 17 x 14 x 45 mm^3 (at 130 mm depth) with a frame rate of 250 Hz led to a system latency of 95.5 ms which is the shortest latency reported so far for MLC tracking. In the literature on electromagnetic transponder-guided MLC tracking, values of 146 ms for the wireless Calypso system[31] (Varian Medical Systems, Palo Alto, CA) and 140 ms for the wired Raypilot[28] (Micropos Medical AB, Gothenburg, Sweden) were reported. Image-guided MLC tracking methods show higher latencies of 264 ms and 382 ms for 5 Hz kV- and MV-imaging, respectively.[36] The 172 ms latency of

300   ultrasound-guided tracking covering a large volume is substantially lower than the other image-guided methods and only slightly higher than the fastest reported methods with electromagnetic transponders. It is also faster than the 2D-2D-ultrasound-guided proton therapy system by Schwaab *et al.* with a reported latency of 200 ms.[23]

It should be noted that the image acquisition time in ultrasound is mainly affected by the number of beams or angles along the up-down and left-right directions within the volume while the scan depth, i.e. the direction away from the

305   probe, has a much smaller effect on the frame rate. Thus, if the probe was aligned with the main motion axis of the tumor, e.g. superior-inferior for many respiratory motions, the volume size could potentially be reduced below the currently chosen 68 mm x 50 mm if the expected residual tumor motion is much less. A lower latency could also reduce latency-related errors which tend to have the highest impact when tracking high-frequency motions, requiring further investigation.[26]

310   While the acoustic mechanisms of image acquisition make ultrasound an attractive modality for real-time, radiation-free imaging, they also cause one of ultrasound's main limitations: speed-of-sound-errors. The ultrasound station calculates distances based on an assumed mean speed of sound in soft tissues (1540 m/s), but different tissue types have different physical properties based on their composition. Inside the body, this can lead to distance errors of up to 7%, i.e. several millimeters.[37] This can currently be compensated retrospectively by correcting the ultrasound volumes

315   via ground-truth density information from CT[38], but no online solution is available. The extent of speed-of-sound errors *in vivo* during tracking still needs to be determined and, if required, compensated for in real-time for accurate absolute target localization in ultrasound.

14

The measured geometric accuracy of sub-1-mm for prostate and sub-2-mm for lung tumor trajectories is well in accordance with reported localization errors of Calypso[34] and image-based tracking methods[39, 40] and only slightly inferior to the reported accuracy of wired transponders (all traces sub-1-mm).[28] All systems except for Calypso are still in the research state and have not been used clinically. The only other study on online ultrasound guidance for radiotherapy reported a geometric error of 4.8 mm, however including an optical calibration of the system to compensate for probe motion.[24] Since the main aim of the current work was to investigate the feasibility of integrating online ultrasound target localization into an existing MLC tracking framework, the "best-case scenario" was chosen: the ultrasound probe was calibrated to the isocenter via the motion stage in accordance with previous studies[27, 31, 39, 41] but kept in a fixed position. The phantom design was minimalistic to assess the highest achievable accuracy. A static systematic offset of -0.4 mm in the SI-direction was observed in the original tracking data. Subtraction of the offset further reduced the total tracking error down to 0.85 mm. It was likely caused by an imperfect alignment of the lead sphere with the isocenter or an unintended and unnoticed shift of the sphere during ultrasound calibration. During calibration, the location of the isocenter is fixed in the ultrasound volume as the tracking origin – an offset would lead to a systematic error in the subsequent measurements.

Assessing the geometric accuracy of ultrasound-guided MLC tracking based on MV portal images in a phantom can be considered an intermediate solution incorporating not only the accuracy of the ultrasound target localization but also errors from the MLC aperture fitting, the tracking latency and the prediction algorithm (lung only). The method determines the geometric error of the entire tracking system in beam's eye view, thus measuring the actual error occurring at treatment delivery.

Dosimetric evaluation of ultrasound-guided MLC tracking yielded a 90% improvement in dose discrepancies from treatments delivered without tracking to deliveries with real-time tracking applied. Treatment efficiency was not reduced by tracking. Over the past years, several MLC tracking studies have used the same treatment plans and trajectories (except for the stable prostate trace).[27, 31, 39, 41] Among these, only Poulsen et al. used kV images for target localization[39] while the other studies used electromagnetic transponders. A dosimetric comparison between the current work and four previous studies can be found in Table 5 (results of the stable trace were removed in the current study for comparability).

All previously conducted studies show similar and substantial dose improvements of 85-95% when MLC tracking is applied, although the pattern of dose errors are different in the two older studies[27, 39] that used a horizontal 2D ion chamber array (PTW Seven29) than in the later studies that used a biplanar diode array (Delta4PT) for dose measurements. While the older studies had highest residual γ-failure rates with tracking for the lung cases, the more recent works including the current study had largest errors for prostate. A potential source of this discrepancy is the

15

difference in the dosimeter geometry. Besides this, larger errors may be expected for kV image-based MLC tracking due to

350   a longer tracking system latency of 290ms[27, 39] as compared to 140-172ms for the other studies.

In the newer studies, the γ-failures with tracking were higher and improvements were lower in the prostate compared with the lung although the geometric tracking error was generally higher for lung traces. There are two factors contributing to these seemingly inconsistent results. First, the geometric and dosimetric measurements were performed in two different experiments which may include different errors and are therefore not directly linked. Second, limitations in

355   the MLC leaf fitting can be assumed to be one of the key contributors for the higher prostate failures. It has previously been shown to be the dominant contributor to MLC tracking errors for prostate motion.[39] If the target moves orthogonally to the MLC leaf direction, the leaf fitting cannot always be optimal due to the finite leaf width. For slow erratic motion, e.g. in the prostate, the target may stay in a position for which the leaves cannot compensate for a relatively long time, thus leading to systematic dose errors with an accumulation of erroneous dose. For faster periodic trajectories, the dose errors caused

360   by leaf fitting will tend to be random and cancel out better. This problem could potentially be overcome by the utilization of thinner MLC leaves or by aligning the MLC with the main motion axis of the target prior or even during the treatment.[42]

Moving towards a clinical implementation of ultrasound-guided MLC tracking, the integration of an external tracking device and the accuracy of a full system calibration will be an integral part of future experiments but may increase

365   the geometric error of the tracking system. Another issue to be addressed is the positioning of the ultrasound probe. For this purpose, we have developed a framework that calculates the expected image quality from a planning CT to optimize probe positions, considering target visibility and treatment beam angles.[43] Due to the high attenuation it has been recommended to avoid beams intersecting with the probe[44], but treatment planning "around the probe" was shown to be feasible in the majority of cases.[45]

370   The construction of a more realistic phantom with reproducible deformations or the utilization of another real-time tracking modality for evaluation is another important precursor for *in vivo* tracking experiments. So far, the accuracy of our real-time tracking system has not been quantified in real patient data. The main reason for that is the lack of a reliable, continuous ground truth. Manual delineation in ultrasound volumes, even when performed by experts, has a high inter- and intra-observer variability[46] while correlation-based techniques only approximate the true target position or

375   provide discrete absolute positions. Using complex phantom and anatomical data with a concomitant ground truth motion signal will also facilitate the development and evaluation of novel algorithms for real-time rotation and deformation tracking.

Even though these initial experiments have been limited to moving phantoms, the chosen trajectories already covered a wide range of real patient motion types. Due to their varying complexity they most likely lead to higher errors

16

than would be expected for typical prostate and lung tumor trajectories.[28] Especially the lung trajectories were chosen for their complex, high-frequency motion patterns to represent the most challenging tracking scenarios with the highest requirement for low latency. While imaging lung tumors with ultrasound for real-time motion compensation will be hardly possible due to the large acoustic impedance mismatch between the air-filled lungs and the surrounding soft tissue, this type of motion is still relevant for targets located in the upper abdomen close to the diaphragm. Suitable regions for ultrasound tracking are for example in the liver, the prostate and also cardiac targets for novel treatment approaches in radiotherapy.[47]

By avoiding ionizing radiation for imaging, having a very high temporal resolution and at the same time producing volumetric anatomical images, ultrasound has striking advantages over other imaging techniques used in radiotherapy. In addition to its demonstrated ability to track three-dimensional translations of rigid target structures non-invasively, it holds the potential to measure target rotations and even deformations in real-time. The capability of detecting such complex target motion raises the demand for sophisticated treatment planning, real-time beam adaptation and online re-optimization techniques. Further progress in these fields, higher computational power as well as new ultrasound systems with improvements in imaging hardware, processing software and research interfaces will all benefit the development of more accurate target localization techniques and pave the way for the integration of real-time ultrasound guidance into the radiotherapy workflow.

Table 5: Dosimetric comparison of different studies on dynamic MLC tracking utilizing the same trajectories and plans as the current study.

Study details	Study	Current study		Hansen et al.[31]		Ravkilde et al.[41]		Poulsen et al.[39]		Keall et al.[27]	
	Guidance method	Ultrasound		Calypso		Raypilot		kV-imaging		Calypso	
	Accelerator	Trilogy		TrueBeam		Trilogy		Trilogy		Trilogy	
	Dosimeter	Delta4PT		Delta4PT		Delta4PT		PTW Seven29		PTW Seven29	
	Tracking type	None	MLC	None	MLC	None	MLC	None	MLC	None	MLC
3%/3mm γ-failures	Lung, high and low modulation combined	19.9%	0.3%	20.4%	0.9%	23.6%	0.2%	41.0%	1.8%	34.0%	1.6%
	Prostate, combined	11.8%	2.9%	14.2%	3.3%	10.7%	2.2%	19.5%	1.4%	14.0%	1.2%
	All combined	15.8%	1.6%	17.3%	2.1%	17.1%	1.2%	30.3%	1.6%	24.0%	1.4%
Improvement from tracking		91%		88%		93%		95%		94%	
2%/2mm γ-failures	Lung, combined	38.0%	1.0%	41.1%	2.4%	46.2%	1.6%	53.5%	7.8%	58.0%	6.6%
	Prostate, combined	26.8%	6.4%	30.4%	8.1%	24.4%	5.8%	33.0%	2.0%	34.0%	5.7%
	All combined	32.4%	3.7%	35.7%	5.3%	35.3%	3.7%	43.3%	4.9%	46.0%	6.1%
Improvement from tracking		90%		85%		89%		89%		86%	

5. CONCLUSION

17

Real-time, online 4D ultrasound tracking was successfully integrated with MLC tracking on a conventional linear accelerator for the first time. It showed similar accuracy and latency as other tracking methods while holding the potential to measure target motion non-invasively. Future efforts will be focused on the non-invasive detection and compensation of target rotation and deformation as well as on the conduction of *in vivo* studies for further validation of the developed tracking framework.

6. ACKNOWLEDGEMENTS

7. CONFLICTS OF INTEREST

The authors have no relevant conflicts of interest to disclose.

REFERENCES

[1]   S.S. Korreman, "Motion in radiotherapy: photon therapy," Phys. Med. Biol. **57**(23), R161–R191 (2012).

[2]   C.X. Yu, D.A. Jaffray, and J.W. Wong, "The effects of intra-fraction organ motion on the delivery of dynamic intensity modulation.," Phys. Med. Biol. **43**(1), 91–104 (1998).

[3]   P.J. Keall, V.R. Kini, S.S. Vedam, and R. Mohan, "Motion adaptive x-ray therapy: a feasibility study.," Phys. Med. Biol. **46**(1), 1–10 (2001).

[4]   P.J. Keall *et al.*, "The management of respiratory motion in radiation oncology report of AAPM Task Group 76.," Med. Phys. **33**(10), 3874–900 (2006).

[5]   J.R. Adler, C. Pham, S.D. Chang, and R.A. Rodas, "Image-guided Robotic Radiosurgery : The CyberKnife," Perspect. Neurosci. (November), (2003).

[6]   K. Takayama *et al.*, "Initial validations for pursuing irradiation using a gimbals tracking system," Radiother. Oncol. **93**(1), 45–49 (2009).

[7]   P.J. Keall *et al.*, "The first clinical implementation of electromagnetic transponder-guided MLC tracking.," Med. Phys. **41**(2), 020702 (2014).

18

[8]   N. Hardcastle *et al.*, "MO-FG-BRA-6: Electromagnetic Beacon Insertion in Lung Cancer Patients and Resultant Surrogacy Errors for Dynamic MLC Tumour Tracking," in *Med. Physics, Accept. Abstr. 58th Annu. Meet. AAPM* (2016).

[9]   Y. Ge, R.T. O'Brien, C.-C. Shieh, J.T. Booth, and P.J. Keall, "Toward the development of intrafraction tumor deformation tracking using a dynamic multi-leaf collimator.," Med. Phys. **41**(6), 061703 (2014).

[10] A. Schweikard, G. Glosser, M. Bodduluri, M.J. Murphy, and J.R. Adler, "Robotic motion compensation for respiratory movement during radiosurgery.," Comput. aided Surg. **5**(4), 263–77 (2000).

[11] T. Mate, D. Krag, J. Wright, and S. Dimmer, "A new system to perform continuous target tracking for radiation and surgery using non-ionizing alternating current electromagnetics," Int. Congr. Ser. **1268**, 425–430 (2004).

[12] S. Mutic and J.F. Dempsey, "The ViewRay System: Magnetic Resonance-Guided and Controlled Radiotherapy," Semin. Radiat. Oncol. **24**(3), 196–199 (2014).

[13] J.J.W. Lagendijk *et al.*, "MRI/linac integration.," Radiother. Oncol. **86**(1), 25–9 (2008).

[14] B.G. Fallone, "The Rotating Biplanar Linac-Magnetic Resonance Imaging System," Semin. Radiat. Oncol. **24**(3), 200–202 (2014).

[15] P.J. Keall, M. Barton, and S. Crozier, "The Australian magnetic resonance imaging-linac program.," Semin. Radiat. Oncol. **24**(3), 203–6 (2014).

[16] T. Bjerre *et al.*, "Three-dimensional MRI-linac intra-fraction guidance using multiple orthogonal cine-MRI planes.," Phys. Med. Biol. **58**(14), 4943–50 (2013).

[17] J. Banerjee, C. Klink, E.D. Peters, W.J. Niessen, A. Moelker, and T. van Walsum, "Fast and robust 3D ultrasound registration - Block and game theoretic matching," Med. Image Anal. **20**(1), 173–83 (2015).

[18] L. Royer, M. Marchal, A. Le Bras, G. Dardenne, and A. Krupa, "Real-time Tracking of Deformable Target in 3D Ultrasound Images," in *IEEE Int. Conf. Robot. Autom. ICRA'15*(Seattle, United States, 2015).

[19] S. Vijayan, S. Klein, E.F. Hofstad, F. Lindseth, B. Ystgaard, and T. Langø, "Motion tracking in the liver: Validation of a method based on 4D ultrasound using a nonrigid registration technique," Med. Phys. **41**(8), 082903 (2014).

[20] E.J. Harris, N.R. Miller, J.C. Bamber, J.R.N. Symonds-Tayler, and P.M. Evans, "Speckle tracking in a phantom and feature-based tracking in liver in the presence of respiratory motion using 4D ultrasound.," Phys. Med. Biol. **55**(12), 3363–3380 (2010).

[21] T.P. O'Shea, L.J. Garcia, K.E. Rosser, E.J. Harris, P.M. Evans, and J.C. Bamber, "4D ultrasound speckle tracking of intra-fraction prostate motion: a phantom-based comparison with x-ray fiducial tracking using CyberKnife.," Phys. Med. Biol. **59**(7), 1701–20 (2014).

[22] M. a Lediju-Bell, B.C. Byram, E.J. Harris, P.M. Evans, and J.C. Bamber, "In-vivo liver tracking with a high volume rate

19

460   4D ultrasound scanner and a 2D matrix array probe," Phys. Med. Biol. **57**(5), 1359–1374 (2012).

[23]   J. Schwaab *et al.*, "Ultrasound tracking for intra-fractional motion compensation in radiation therapy," Phys. Medica **30**(5), 578–582 (2014).

[24]   J. Schwaab *et al.*, "First Steps Toward Ultrasound-Based Motion Compensation for Imaging and Therapy: Calibration with an Optical System and 4D PET Imaging," Front. Oncol. **5**(November), 1–10 (2015).

465 [25]   K. V. Mackenzie, "Discussion of sea water sound-speed determinations," J. Acoust. Soc. Am. **70**(3), 801 (1981).

[26]   P.R. Poulsen, B. Cho, A. Sawant, D. Ruan, and P.J. Keall, "Dynamic MLC tracking of moving targets with a single kV imager for 3D conformal and IMRT treatments.," Acta Oncol. **49**(7), 1092–1100 (2010).

[27]   P.J. Keall *et al.*, "Electromagnetic-guided dynamic multileaf collimator tracking enables motion management for intensity-modulated arc therapy," Int. J. Radiat. Oncol. Biol. Phys. **79**(1), 312–320 (2011).

470 [28]   T. Ravkilde, P.J. Keall, K. Højbjerre, W. Fledelius, E. Worm, and P.R. Poulsen, "Geometric accuracy of dynamic MLC tracking with an implantable wired electromagnetic transponder.," Acta Oncol. **50**, 944–951 (2011).

[29]   Y. Suh, S. Dieterich, B. Cho, and P.J. Keall, "An analysis of thoracic and abdominal tumour motion for stereotactic body radiotherapy patients," Phys. Med. Biol. **53**(13), 3623–3640 (2008).

[30]   K.M. Langen *et al.*, "Observations on Real-Time Prostate Gland Motion Using Electromagnetic Tracking," Int. J.
475   Radiat. Oncol. **71**(4), 1084–1090 (2008).

[31]   R. Hansen *et al.*, "Electromagnetic guided couch and multileaf collimator tracking on a TrueBeam accelerator," Med. Phys. **43**(5), 2387–2398 (2016).

[32]   K. Malinowski *et al.*, "Development of the 4D Phantom for patient-specific, end-to-end radiation therapy QA," in *Proc. SPIE 6510, Med. Imaging 2007 Phys. Med. Imaging*, edited by J. Hsieh and M.J. Flynn (San Diego, CA, 2007), p.
480   65100E.

[33]   D. Ruan, "Kernel density estimation-based real-time prediction for respiratory motion," Phys. Med. Biol. **55**(5), 1311–1326 (2010).

[34]   A. Sawant *et al.*, "Toward Submillimeter Accuracy in the Management of Intrafraction Motion: The Integration of Real-Time Internal Position Monitoring and Multileaf Collimator Target Tracking," Int. J. Radiat. Oncol. Biol. Phys.
485   **74**(2), 575–582 (2009).

[35]   P.R. Poulsen, B. Cho, A. Sawant, D. Ruan, and P.J. Keall, "Detailed analysis of latencies in image-based dynamic MLC tracking.," Med. Phys. **37**(9), 4998–5005 (2010).

[36]   W. Fledelius *et al.*, "Tracking latency in image-based dynamic MLC tracking with direct image access.," Acta Oncol. **50**(6), 952–959 (2011).

490 [37]   D. Fontanarosa, S. van der Meer, E. Bloemen-van Gurp, G. Stroian, and F. Verhaegen, "Magnitude of speed of sound

aberration corrections for ultrasound image guided radiotherapy for prostate and other anatomical sites.," Med. Phys. **39**(8), 5286–92 (2012).

38   D. Fontanarosa, S. van der Meer, E. Harris, and F. Verhaegen, "A CT based correction method for speed of sound aberration for ultrasound based image guided radiotherapy.," Med. Phys. **38**(5), 2665–2673 (2011).

39   P.R. Poulsen, W. Fledelius, B. Cho, and P. Keall, "Image-Based Dynamic Multileaf Collimator Tracking of Moving Targets During Intensity-Modulated Arc Therapy," Radiat. Oncol. Biol. **83**(2), e265–e271 (2012).

40   P.R. Poulsen *et al.*, "Megavoltage image-based dynamic multileaf collimator tracking of a NiTi stent in porcine lungs on a linear accelerator.," Int. J. Radiat. Oncol. Biol. Phys. **82**(2), e321–7 (2012).

41   T. Ravkilde, P.J. Keall, C. Grau, M. Høyer, and P.R. Poulsen, "Time-resolved dose distributions to moving targets during volumetric modulated arc therapy with and without dynamic MLC tracking," Med. Phys. **40**(11), 111723 (2013).

42   K. Otto and B.G. Clark, "Enhancement of IMRT delivery through MLC rotation," Phys. Med. Biol. **47**(22), 3997–4017 (2002).

43   R. Gong, R. Bruder, A. Schweikard, J. Schlosser, and D. Hristov, "Augmented reality system for ultrasound-guided radiation therapy," Int. J. Comput. Assist. Radiol. Surg. - Proc. 29th Int. Congr. Exhib. Barcelona, Spain **10**(1, Supplement), 39–40 (2015).

44   M. Bazalova-Carter, J. Schlosser, J. Chen, and D. Hristov, "Monte Carlo modeling of ultrasound probes for image guided radiotherapy," Med. Phys. **42**(10), 5745–5756 (2015).

45   Y. Zhong, K.L. Stephans, P. Qi, N. Yu, J. Wong, and P. Xia, "Assessing Feasibility of Real-time Ultrasound Monitoring in Stereotactic Body Radiotherapy of Liver Tumors," Technol. Cancer Res. Treat. **12**(3), 243–250 (2013).

46   V. De Luca *et al.*, "The 2014 liver ultrasound tracking benchmark," Phys. Med. Biol. **60**(14), 5571–5599 (2015).

47   R. Bruder, T. Cai, F. Ernst, and A. Schweikard, "3D ultrasound-guided motion compensation for intravascular radiation therapy," in *Proc. 23rd Int. Conf. Exhib. Comput. Assist. Radiol. Surg.*(International Journal of Computer Assisted Radiology and Surgery, 2009), pp. 22–28.

(a)

MLC aperture
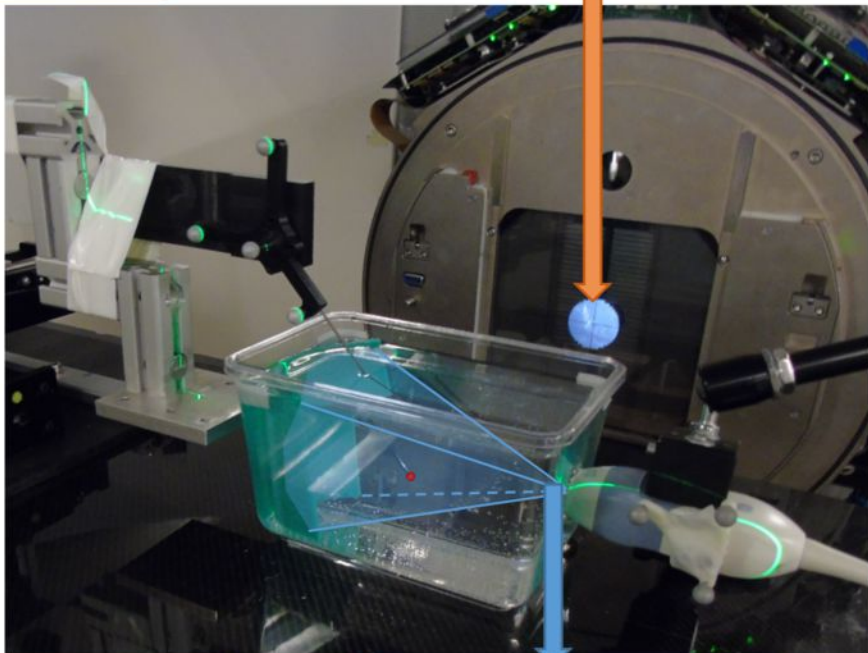
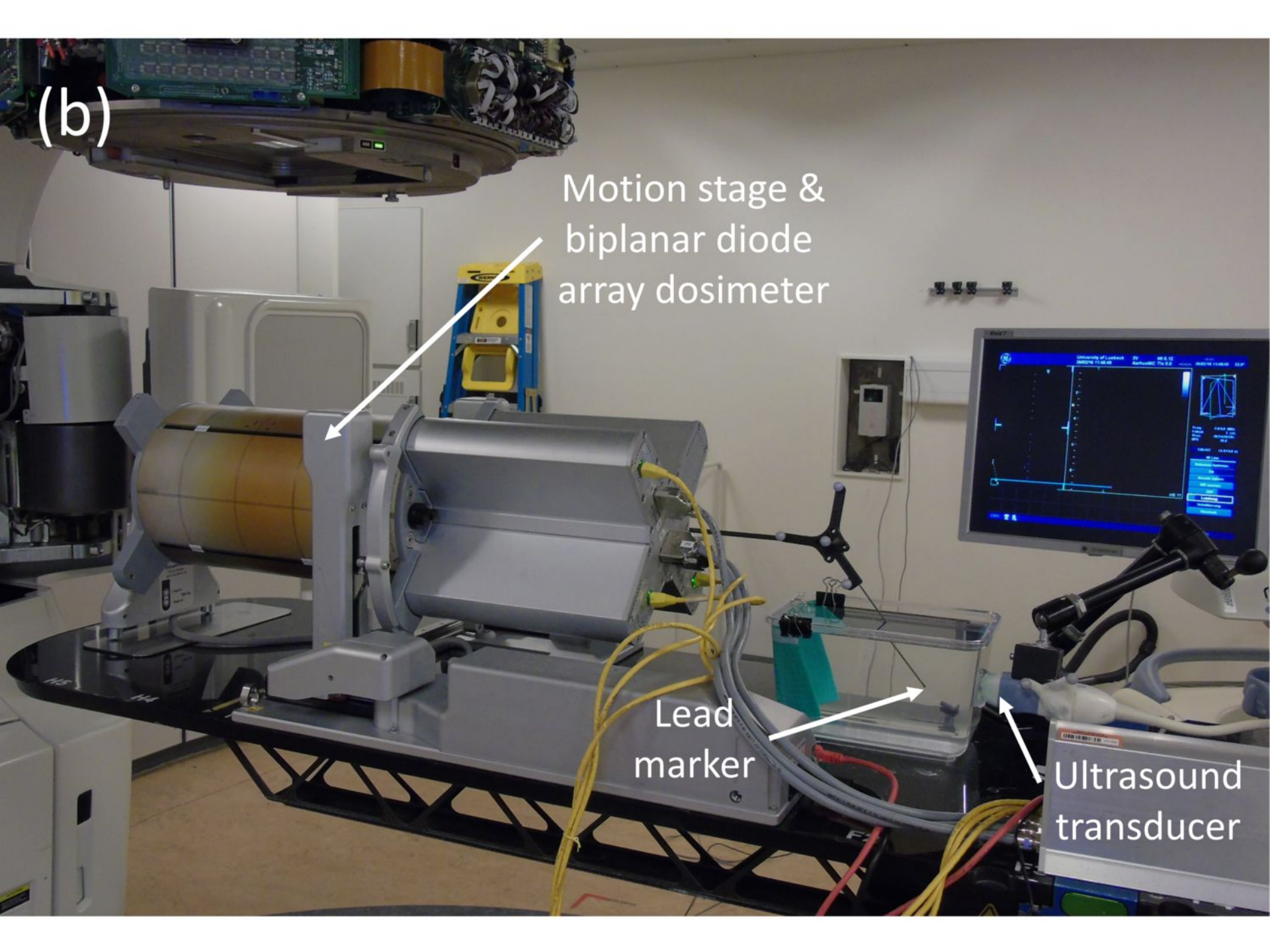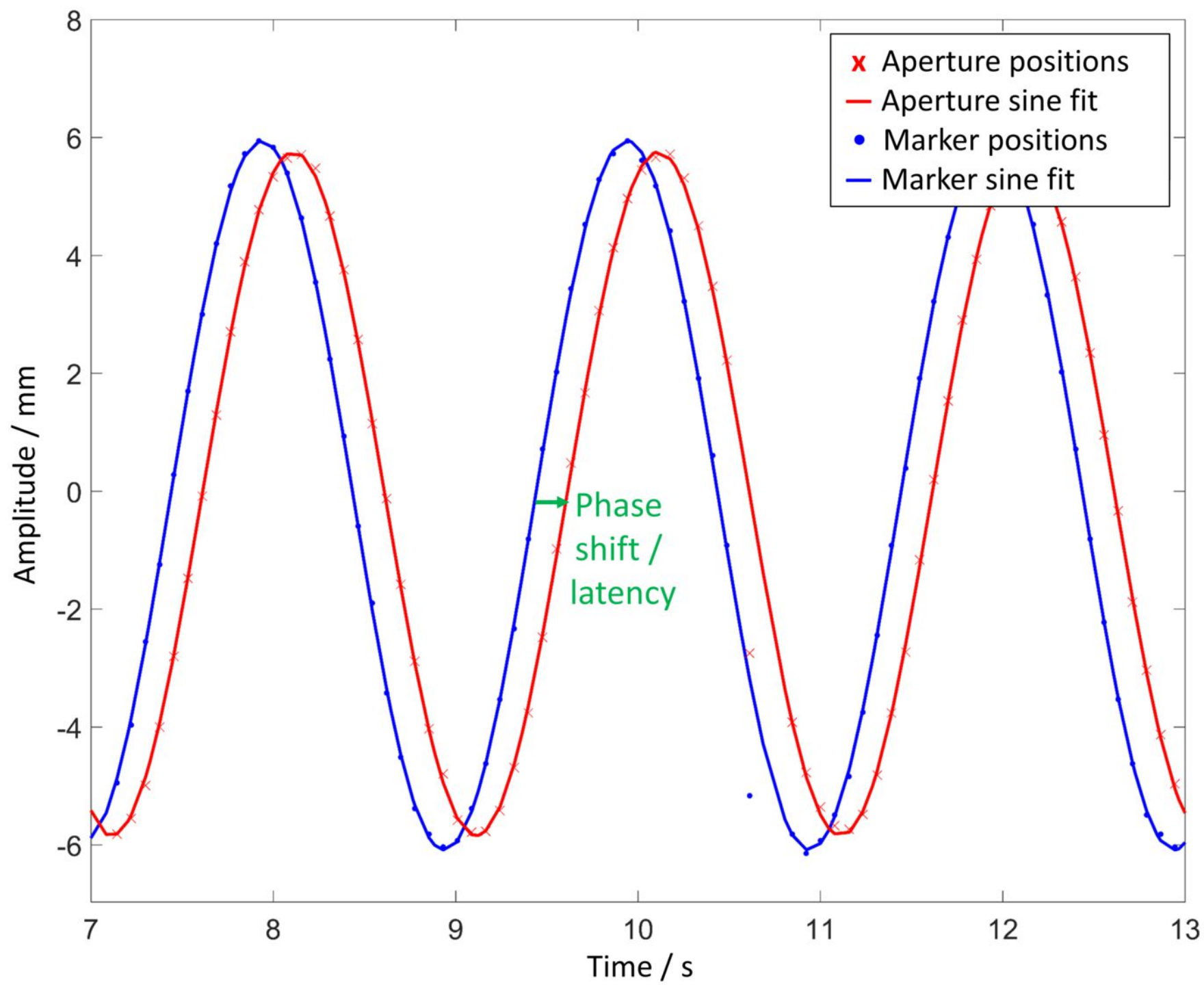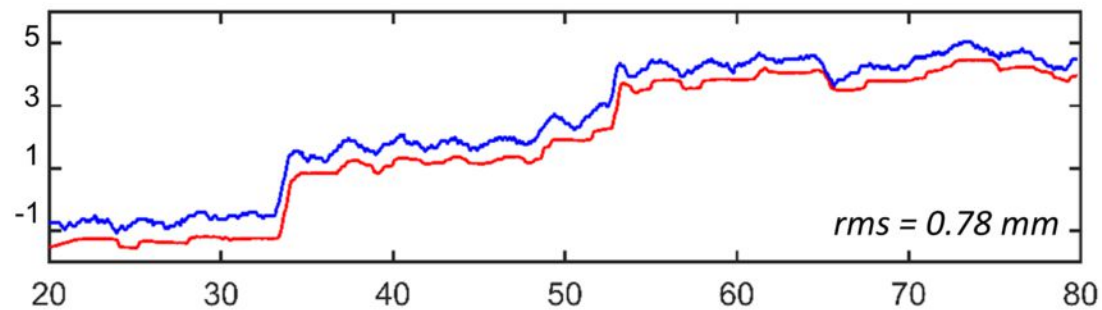Motion stage

Lead marker

Ultrasound transducer
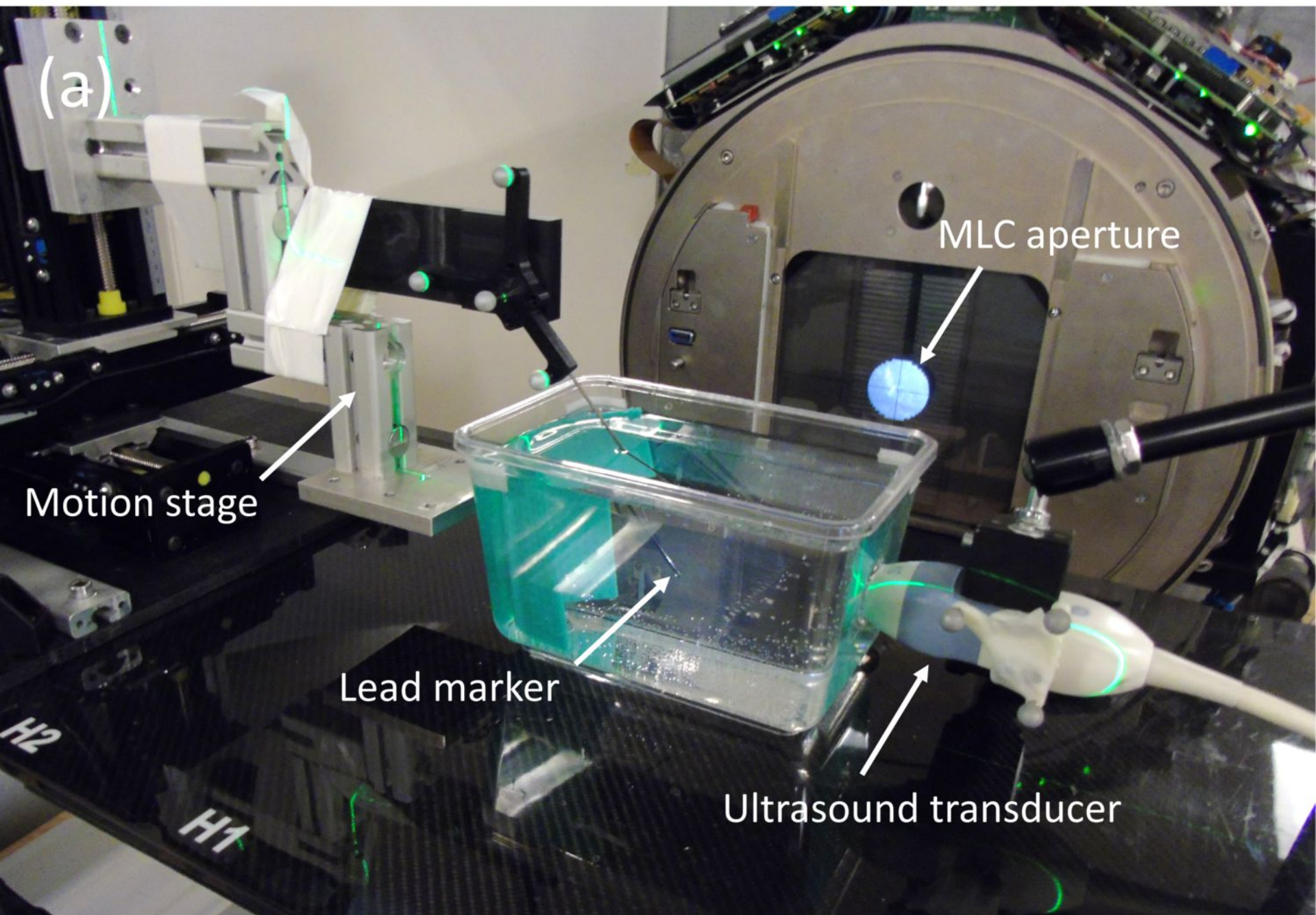
(b)

Motion stage & biplanar diode array dosimeter

Lead marker

Ultrasound transducer

Before offset correction (original data) — After offset correction
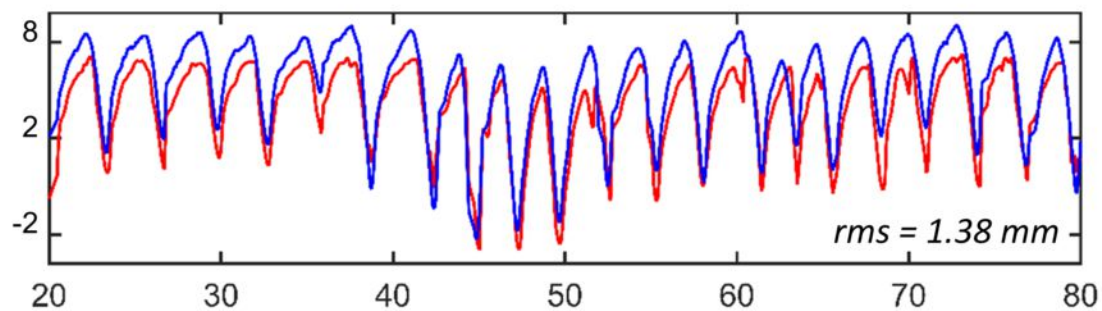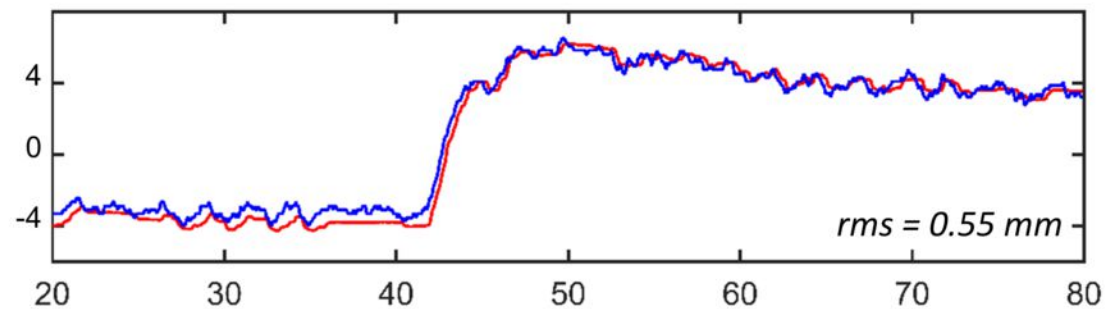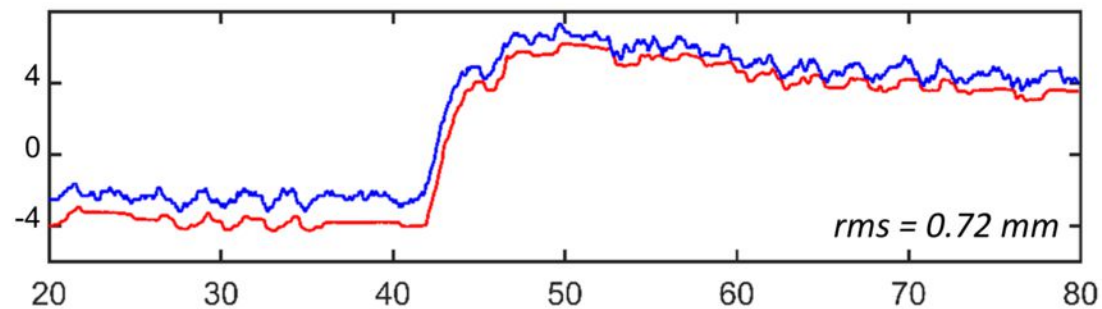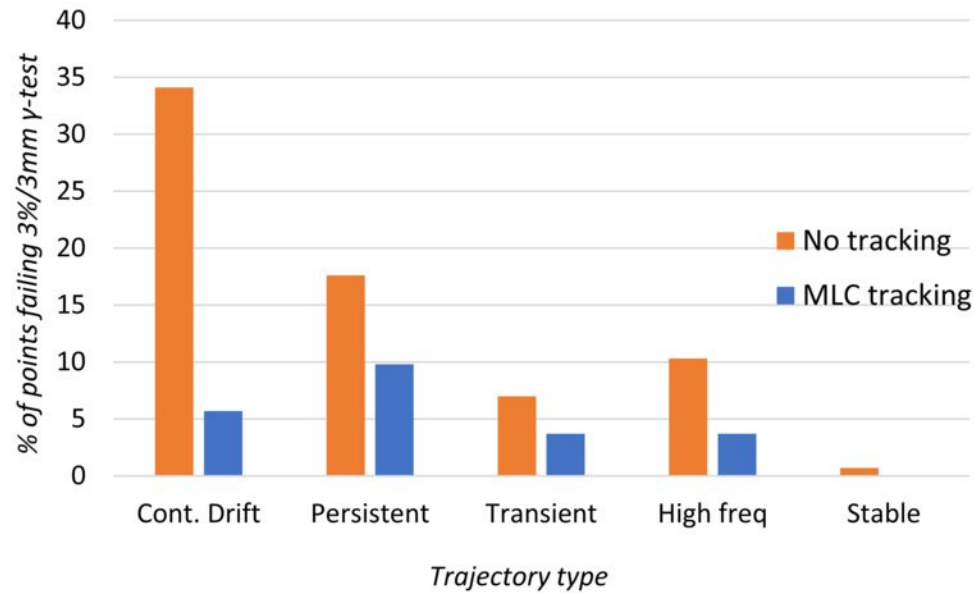
Prostate continuous drift — Prostate persistent excursion — Lung typical motion

rms = 0.78 mm, rms = 0.55 mm, rms = 0.72 mm, rms = 0.55 mm, rms = 1.38 mm, rms = 1.13 mm

SI position (1D) / mm vs Time / s
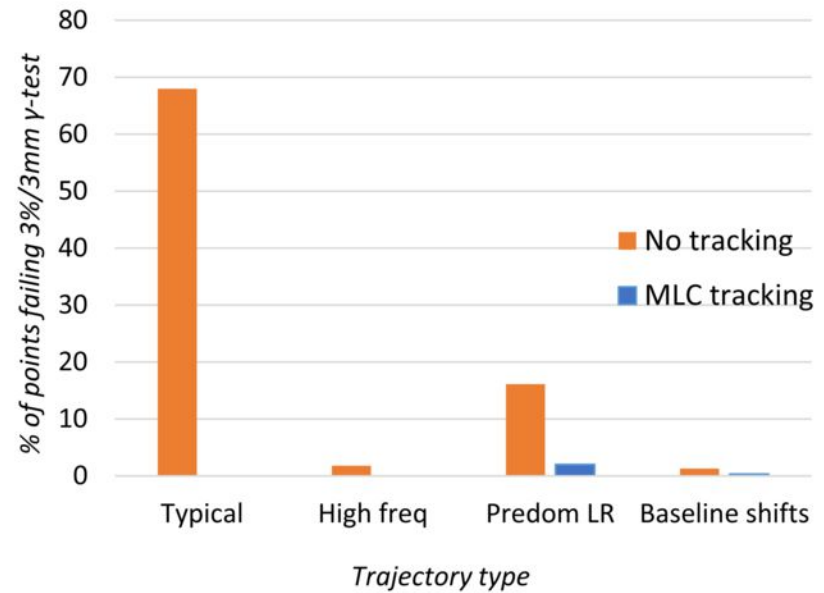
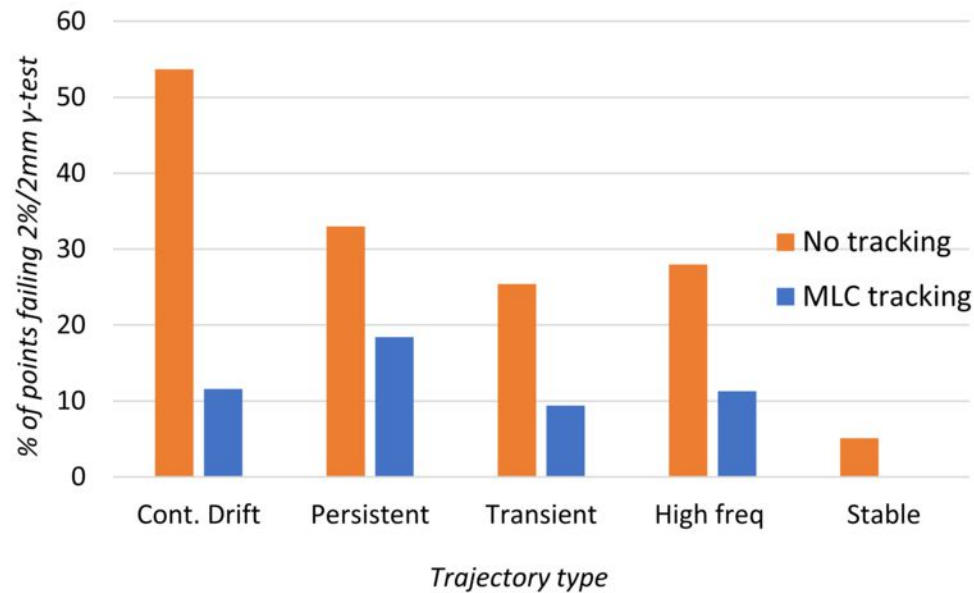Aperture position (red), Marker position (blue)
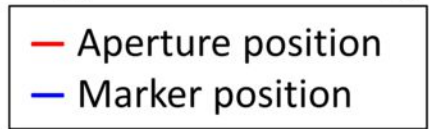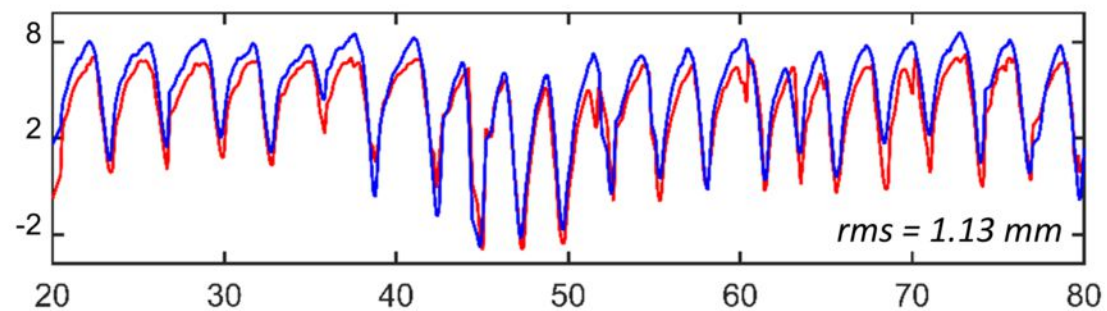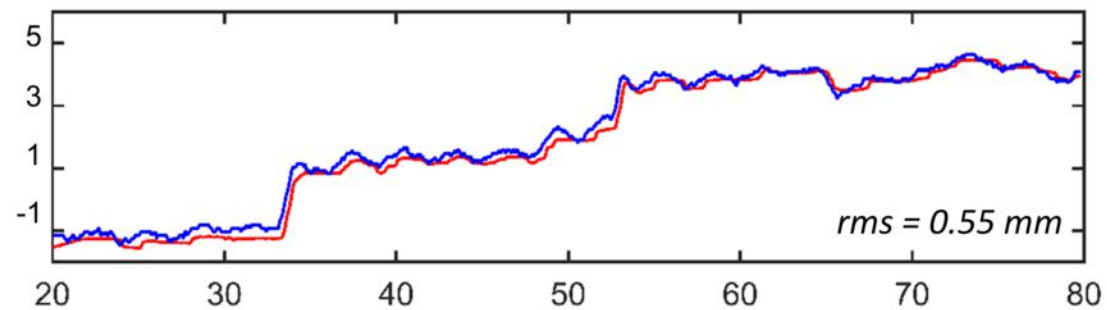
Prostate 3% / 3 mm γ-failure rates

Lung 3% / 3 mm γ-failure rates

Prostate 2% / 2 mm γ-failure rates

Lung 2% / 2 mm γ-failure rates